Structure of TRPV1 channel revealed by electron cryomicroscopy

Vera Y. Moiseenkova-Bell*, Lia A. Stanciu†, Irina I. Serysheva*, Ben J. Tobe*, and Theodore G. Wensel*‡

*Verna and Marrs McLean Department of Biochemistry and Molecular Biology, Baylor College of Medicine, Houston, TX 77030; and †Department of Materials Science and Engineering, Purdue University, West Lafayette, IN 47907

Edited by Clara Franzini-Armstrong, University of Pennsylvania School of Medicine, Philadelphia, PA, and approved March 6, 2008 (received for review December 16, 2007)

The transient receptor potential (TRP) family of ion channels participate in many signaling pathways. TRPV1 functions as a molecular integrator of noxious stimuli, including heat, low pH, and chemical ligands. Here, we report the 3D structure of full-length rat TRPV1 channel expressed in the yeast *Saccharomyces cerevisiae* and purified by immunoaffinity chromatography. We demonstrate that the recombinant purified TRPV1 channel retains its structural and functional integrity and is suitable for structural analysis. The 19-Å structure of TRPV1 determined by using single-particle electron cryomicroscopy exhibits fourfold symmetry and comprises two distinct regions: a large open basket-like domain, likely corresponding to the cytoplasmic N- and C-terminal portions, and a more compact domain, corresponding to the transmembrane portion. The assignment of transmembrane and cytoplasmic regions was supported by fitting crystal structures of the structurally homologous Kv1.2 channel and isolated TRPV1 ankyrin repeats into the TRPV1 structure.

cryoelectron microscopy | ion channels | TRP channels

The transient receptor potential (TRP) family of cation channels, named for a *Drosophila* mutant with defective vision (1, 2) characterized by a *t*ransient *r*eceptor *p*otential, consist of seven major branches in metazoans: TRPV, TRPA, TRPC, TRPM, TRPP, TRPML, and TRPN (3). These channels have diverse properties with respect to gating and ion selectivity, and in the few cases where they are known, diverse physiological functions (4). Some TRP channels respond to physical stimuli such as heat, cold, or osmotic stress, and some are gated by pH changes in the physiological range (5, 6). They are thought in many cases to be coupled to signaling by G protein-coupled receptors, as in invertebrate vision, where they serve as the transduction channels (7). All are predicted to have six transmembrane helices per subunit, with varying sizes of cytoplasmic N and C termini, and all are proposed to form tetrameric assemblies (8).

TRPV1, previously known as VR1 for vanilloid receptor one, was identified as the receptor for the vanilloid compound, capsaicin, the active ingredient in hot chili peppers (9). TRPV1 is expressed in polymodal nociceptors and is believed to function as a molecular integrator of noxious stimuli, including heat, vanilloids, acids, and endogenous proinflammatory substances (*N*-arachidonoyldopamine, lipoxygenase products of arachidonic acid, and anandamide) (10–13).

Rat TRPV1 is a 95-kDa integral plasma membrane protein of 838 aa per subunit predicted to have a transmembrane region formed by residues 433–684 consisting of six transmembrane helical segments, S1–S6, plus a "P-loop," which together with transmembrane helices S5 and S6 is thought to form the ion pore and selectivity filter based on homology with other ion channels (9, 14). The rest of the protein including intracellular N- and C-terminal sequences forms the large cytoplasmic region and comprises ≈70% of the protein mass. TRPV1 functions as a nonselective tetrameric cation channel with a high permeability to calcium (permeability sequence $Ca^{2+} > Mg^{+2} > Na^{+} \approx K^{+} \approx Cs^{+}$) (15, 16).

Despite the intense interest in TRP channels generally, and TRPV1 in particular, no 3D structure of the full-length TRPV1 channel has been available.

In this study, to understand the structural motifs characteristic of TRP channels, we have solved the structure of a full-length TRPV1 channel at 19-Å resolution by single-particle electron cryomicroscopy (cryo-EM). To do this, we developed a procedure for overexpression and purification of recombinant mammalian TRPV1 from yeast. Importantly, the structural and functional integrity of the recombinant protein was established by gel-filtration chromatography and ligand-gated Ca^{2+} flux assays. We find that the TRPV1 structure is consistent with those of other tetrameric six-transmembrane-segment channels, conforming to a two-domain motif referred to as a "hanging gondola" (17–21).

Results

Overexpression and Purification of Tetrameric TRPV1. To perform structural analysis of TRPV1, we used a yeast expression system shown to produce functional channels that allowed Ca^{2+} entry when activated by capsaicin and that bound the specific ligand, resiniferatoxin (RTX) (22). To improve the efficiency of purification, we used an epitope tag that has been successfully used to purify a variety of transmembrane proteins, the 1D4 epitope from the C terminus of the G protein-coupled receptor rhodopsin (23, 24). The nonapeptide epitope tag incorporated into the C terminus of TRPV1 allowed us to purify TRPV1 in a single step using an immobilized monoclonal antibody, 1-D4 (Fig. 1*a*). A typical yield from this procedure is 1.5 mg of purified protein per 15 liters of cultured cells. Two bands were detected in Coomassie-blue-stained SDS/PAGE of TRPV1 (Fig. 1*a*) purified from yeast by using an immobilized 1D4 column and peptide elution: a major band with an apparent mass of 106 kDa, and a minor band of 98 kDa that constitutes 5–10% of the entire protein. Immunoblots (Fig. 1*a*) revealed that both bands are due to recombinant TRPV1 protein with intact C-terminal epitope tags. Treatment with peptide-*N*-glycosidase F (PNGase F), which cleaves N-glycosidic bonds between the sugar portion and asparagine of glycoproteins, did not shift the upper band to the position of the lower one, and treatment of yeast cells with tunicamycin slowed growth and reduced protein expression but did not affect the relative levels of the two bands. Therefore, we conclude that the size heterogeneity is unlikely to be due to

Author contributions: V.Y.M.-B. and T.G.W. designed research; V.Y.M.-B. and L.A.S. performed research; V.Y.M.-B. and B.J.T. contributed new reagents/analytic tools; V.Y.M.-B., L.A.S., I.I.S., and T.G.W. analyzed data; and V.Y.M.-B., I.I.S., and T.G.W. wrote the paper.

The authors declare no conflict of interest.

This article is a PNAS Direct Submission.

‡To whom correspondence should be addressed at: Department of Biochemistry and Molecular Biology, Baylor College of Medicine, One Baylor Plaza, Houston, TX 77030. E-mail: twensel@bcm.tmc.edu.

This article contains supporting information online at www.pnas.org/cgi/content/full/0711835105/DCSupplemental.

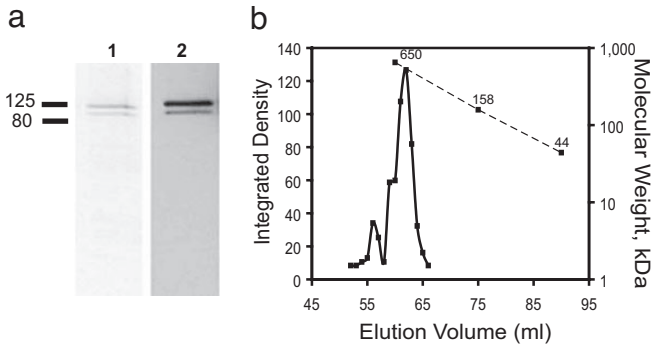

Fig. 1. Purification of TRPV1 from *S. cerevisiae* membranes. (*a*) SDS/PAGE analysis of TRPV1 eluted from an immunoaffinity column (lane 1) and Western blotting of the elution fraction with 1D4 antibody (lane 2). The minor lower band contains the C-terminal 1D4 epitope and may result from proteolysis at the N terminus. (*b*) Representative gel-filtration trace of TRPV1 on Superdex 200 HiLoad 16/60 column. The migration positions of molecular mass standards (dashed line) and a least-squares fit of elution volume (solid line) vs. molecular mass are shown. Amounts of TRPV1 in each fraction were determined by Western blot analysis with 1D4 antibody. The calculated molecular mass of TRPV1 including bound detergent is ≈500 kDa, in good agreement with the position of the major peak. Sizes of molecular mass standards are shown on the plot (650, 158, and 44 kDa).

heterogeneous glycosylation and is likely due to proteolytic removal of an ≈10-kDa N-terminal peptide. The presence of 5–10% of cleaved protein is not likely to have a significant effect on the 3D structure determined by using a single-particle cryo-EM approach.

A tetrameric state of the purified channel protein was confirmed by using size-exclusion chromatography (Fig. 1*b*). The narrowness of the major tetrameric peak eluted from the gel-filtration column suggests that the assembled channel subunits in this peak are monodisperse, properly folded protein particles with an apparent molecular mass of 498 kDa, corresponding to the correct size of the tetrameric channel plus 30% additional mass due to carbohydrate modifications and bound detergent.

Functionality of Purified TRPV1. In previous work, the functionality of yeast-expressed TRPV1 was shown by capsaicin-induced calcium influx in yeast expressing the mammalian channel (22). To test the functionality of the purified protein, Ca^{2+}-flux measurements were performed with TRPV1 channels reconstituted into unilamellar vesicles. The external Ca^{2+} from the vesicles solution was removed by sequential gel filtration and treatment with a "calcium sponge" chelating resin (25) to reduce contaminating metal ions to low nanomolar levels. To activate TRPV1, we used the naturally occurring high-affinity agonist, resiniferatoxin (RTX) (11). The Fura-2 excitation spectra in Fig. 2 *a* and *b* show that before agonist addition the suspension of TRPV1-containing vesicles and control protein-free vesicles had very low levels of residual external Ca^{2+}. When 50 nM RTX was added to TRPV1-containing vesicles, Ca^{2+} was rapidly released, within the manual mixing time, immediately shifting the excitation spectrum of the dye toward that of the Ca^{2+}-bound form. In contrast, RTX did not have a detectable effect on the excitation spectrum of the dye solution in which the control vesicles were suspended, ruling out Ca^{2+} contamination or a direct effect on bilayer Ca^{2+} permeability as the source of the agonist effect on Fura-2 fluorescence (Fig. 2*b*). The spectra shown are representative of six experiments in which, on average (±SEM), 16.8% (±3.2%) of total vesicular calcium was released by RTX from TRV1-containing vesicles, and 1.2% (±0.09%) was released from protein-free control vesicles ($P < 0.001$) [see supporting information (SI) Fig. S1].

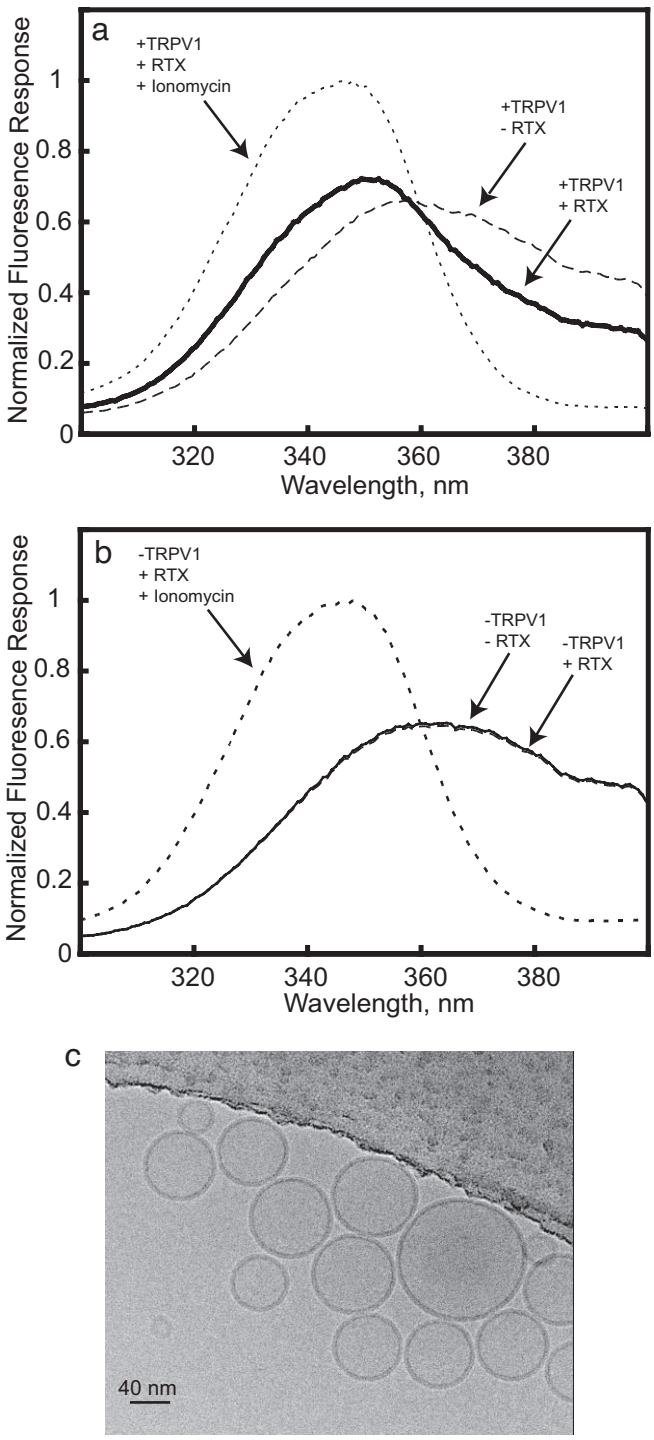

Fig. 2. Agonist-induced Ca^{2+} efflux from TRPV1 vesicles. (*a*) Fura-2 excitation spectra measured before (dashed line) and immediately after (solid line) application of 50 nM resiniferotoxin (RTX) to the cuvette containing TRPV1 vesicles loaded with 5 mM internal Ca^{2+}. Ionomycin (2 μM) induced changes represented by the small-dashed line. (*b*) The same experiment with protein-free vesicles prepared identically but without TRPV1 reveals no release of Ca^{2+} by RTX ($n = 6$). (*c*) Image of TRPV1 vesicles.

Thus, the purified, reconstituted TRPV1 is able to bind RTX and conduct Ca^{2+}, as expected for a fully functional channel. This assay provides a means to test functionality of wild-type or mutant TRPV1, and because it is fluorescence based, should be readily adaptable to high-throughput screens. Addition of the

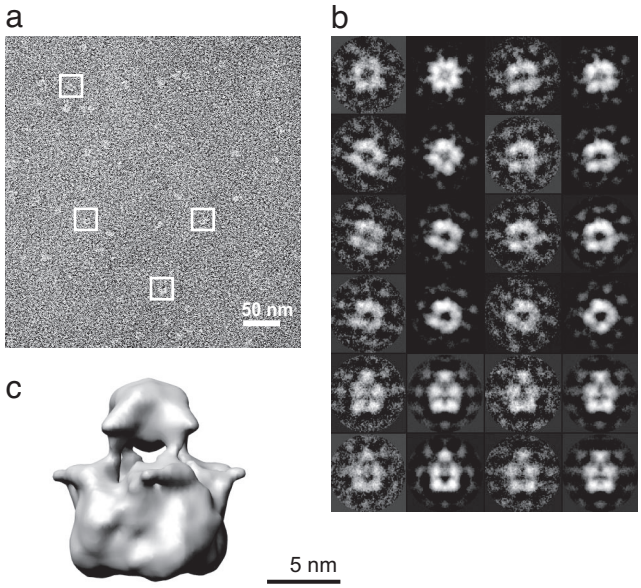

Fig. 3. Single-particle electron microscopy of TRPV1. (*a*) Typical field from a raw image of a frozen solution of the channel, with individual protein images, or particles, surrounded by white rectangles. (*b*) Comparison of class-averaged images (second and fourth columns) with projections of the final 3D model (first and third columns). (*c*) Three-dimensional map of TRPV1 in an isosurface representation with the contour level chosen to enclose a molecular volume corresponding to a mass of 500 kDa.

Ca^{2+} ionophore, ionomycin, to the vesicles (Fig. 2) revealed that a substantial portion of the entrapped Ca^{2+} was still sequestered within vesicles after TRPV1 activation. We repeated this experiment, carefully quantifying the protein:lipid ratio and mean vesicle area (see *Materials and Methods*) so that we could calculate the fraction of vesicles with and without inserted channels. In those experiments (data not shown), 14.8% of the total releasable Ca^{2+} was released by RTX, whereas 20.5% of the vesicles were estimated to contain TRPV1. Thus, at least 72% of the channels are active; this number is a lower limit because the TRPV1-containing vesicles are likely more leaky than those without protein, so these results are consistent with nearly all of the purified channels being functional.

Visualization and Structural Features in Three-Dimensional Reconstruction of TRPV1. A representative section of an electron micrograph of ice-embedded TRPV1 channel is shown Fig. 3*a*. Images show individual molecules in what appears to be a random distribution on the grid: depending on their orientation in the layer of vitreous ice, the TRPV1 channel particles appeared as either square-like projections with a central depression or approximately trapezoidal-shaped projections with variable density distribution. This observation was further confirmed through image processing (Figs. 3*b* and 4). The fourfold symmetry was clearly revealed (see Fig. S2) in class-averages generated during the initial steps of image analysis without imposing symmetry (26).

The 3D structure of TRPV1 (Fig. 3*c*) is 150 Å tall and consists of two major regions with nearly square cross-sections connected via four bridging densities. The corners of the squares and the points of contact with the bridging densities are rotated ≈35° with respect to each other (the hand of the rotation is assigned arbitrarily). The small region is compact and comprises 30% of the total volume. It has dimensions of 60 Å × 60 Å and a height of 40 Å. The large region comprising 70% of the total mass is basket-like, containing a large open volume in its center.

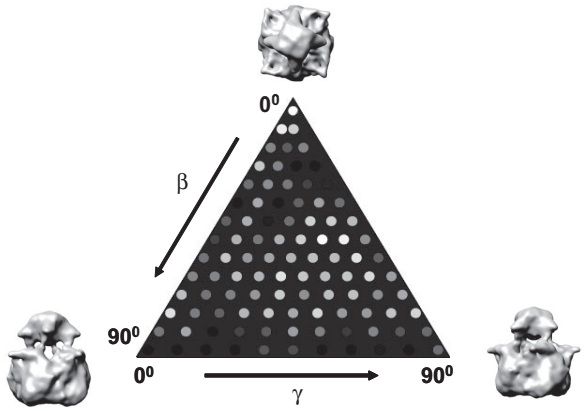

Fig. 4. Distribution of particle orientations over the asymmetric unit used in the reconstruction. Brighter dots denote a larger number of particles (minimum 35; maximum 200).

It measures 100 Å on a side and has a height of 110 Å. The central floor of the basket is only 18 Å thick. The large region has four radial protuberances that are twisted with respect to those of the smaller region.

The relative volumes estimated for large and small regions by using the isosurface shown in Fig. 3*c* are in good agreement with those expected from the sequence prediction for the cytoplasmic and transmembrane regions (70% and 30%, respectively) of the channel protein. We therefore propose that the larger basket-like region is cytoplasmic, containing the N and C termini of the channel protein, including the N-terminal ankyrin repeats and the "tetramerization domain" of the C termini; the smaller region contains the membrane-spanning parts of the four TRPV1 channel subunits as indicated by the proposed position of the lipid bilayer in Fig. 5. This topological assignment of two major channel regions with respect to the membrane is consistent with visualization of continuous densities within the smaller compact region that are sufficient to span the lipid bilayer and are large enough to encompass six transmembrane segments from each protein monomer, as shown in the cutaway view in Fig. 5. In contrast, the basket-like region exhibits a quite hollow appearance and lacks a central portion thick enough to form the ion conduction pathway across the phospholipid bilayer.

A similar two-domain arrangement referred to as a "hanging gondola" has been observed in 3D structures of K channels (17–19) and the cyclic nucleotide-gated channels (20, 21), in which the cytoplasmic region "hangs" underneath the transmembrane domain of the channel.

Comparison with Other Channel Structures. Fig. 6 compares the architecture of the TRPV1 channel with that of the one eukary-

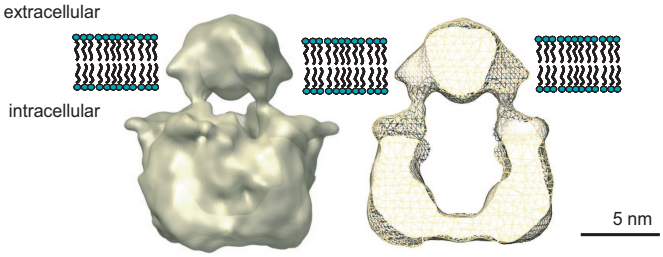

Fig. 5. The proposed location of the 3D structure of TRPV1 in the plasma membrane. A vertical cut-away view shows the internal mass distribution of the protein.

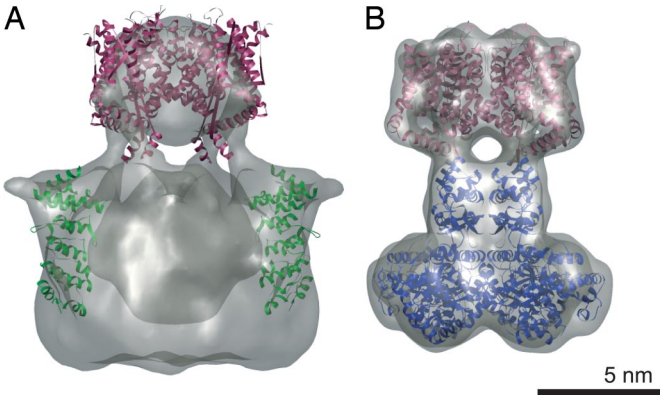

Fig. 6. Comparison of 3D reconstruction of TRPV1 to atomic structures of Kv1.2 potassium channel and TRPV1 ankyrin repeats. (*a*) Docking of the high-resolution structure of Kv1.2 transmembrane domains (maroon; PDB entry 2A79) and TRPV1 ankyrin domains (green; PDB entry 2PNN; two of four such domains are shown) into TRPV1 3D reconstruction. (*b*) Representation of x-ray structure of Kv1.2 (PDB entry 2A79) at 19-Å resolution (maroon, transmembrane domains; blue, T1 domain and β-subunit).

otic tetrameric channel protein for which a high-resolution structure is available, Kv 1.2 (27). The predicted topology of TRP channels has been proposed to resemble that of voltage-gated potassium channels (3, 8), based on biochemical and mutagenesis data. These channels include intracellular N- and C-terminal regions of variable length and six membrane-spanning helices with the "P-loop" pore-forming segment consisting of a short helix and loop between transmembrane helices 5 and 6. In addition to a similar predicted secondary structure and topology in the transmembrane domain, TRPV1 is a tetramer (based on the size and symmetry we observe) as observed for potassium channels.

Other eukaryotic homotetrameric ion channels have a two-layer architecture with distinct cytoplasmic and membrane-embedded domains, including potassium channels, the $InsP_3$ receptor, and the ryanodine receptor (28–33).

Because of their similar topologies and symmetries, we asked how well the crystal structure of the Kv1.2 potassium channel (27) fits into the map for TRPV1 (Fig. 6). Kv1.2 has six segments per transmembrane subunit and forms a tetramer. The size and shape of the transmembrane region of Kv1.2 manually fit well with the portion of the TRPV1 map assigned as the likely transmembrane domain, and the two layer architectures are qualitatively similar, supporting the assignment of the N- and C-terminal domains to the hanging basket.

Recently, structures of TRPV1 and TRPV2 ankyrin repeat domains were solved (34–36). The N-terminal cytoplasmic portion contains ankyrin repeats that are thought to be important for protein function, and it was suggested that the flexible structures of ankyrin domains can provide excellent scaffolds for protein–protein interaction and that they bind the channel modulators, ATP and calmodulin (36). We fitted the structures of the ankyrin repeats that have been solved for TRPV1 (36) into the 3D map of TRPV1 (Fig. 6) and found that they fit well into densities in the proposed cytoplasmic domains. Although further evidence is needed to confirm this location for the ankyrin repeats of TRPV1, it is consistent with current results and would provide an accessible location for interactions with other proteins at the interface between the cytoplasm and membrane surface.

Discussion

Here, we report the structure of TRPV1 determined by using single-particle electron cryomicroscopy. It exhibits fourfold symmetry and comprises two distinct regions: a large open basket-like domain, likely corresponding to the cytoplasmic N- and C-terminal portions, and a more compact domain, corresponding to the transmembrane portion. Assignment of these regions was supported by fitting crystal structures of the structurally homologous Kv1.2 channel and isolated TRPV1 ankyrin repeats into the TRPV1 cryo-EM structure.

Recently, a cryo-EM study of TRPC3 was reported (37). Surprisingly, the structure described is a very open wireframe-like structure, with overall volume exceeding that of much larger proteins, such as the $InsP_3$ receptor (1,252 kDa, vs. 383 kDa for TRPC3), and with insufficient continuous density to form an obvious transmembrane channel domain. It bears little resemblance to a structure derived from electron microscopy of TRPC3 in negative stain by the same group (38), although the latter is strikingly similar to their bullet-shaped negative-stain structures of TRPM2 (689 kDa) (39), and the unrelated membrane protein, prestin (326 kDa) (40). Based on our preliminary results with TRPV2 and TRPY1, a yeast channel related most closely to the TRPC family among mammalian channels, it seems likely that the structures of TRP channels in general follow the basic structural organization described here for TRPV1.

The cryo-EM map of TRPV1 combined with multiresolution information from other ion channels provides a working model to be tested and refined by additional studies. Further understanding of the structural bases of TRPV1 function will require improving the resolution of the map, identifying the locations of residues with known functions, and observing the structure in different functional states. The structure reported here and the ability to produce substantial amounts of purified recombinant channel protein in functional form set the stage for further studies along these lines for TRPV1 as well as other channels of the TRP family. In addition, our procedure for protein purification and reconstitution allows the functional properties of the channel to be studied in membranes with completely defined protein and lipid compositions.

Materials and Methods

Protein Expression and Purification. The original rat TRPV1 cDNA was a generous gift from David Julius (University of California, San Francisco). The cDNA clone was modified by PCR to include restriction enzyme sites, SpeI at the 5′ end and MluI at the 3′ end. A 1D4 immunoaffinity tag (TETSQVAPA) was added to the C terminus to enable purification. This construct was subcloned into the yeast expression plasmid YEpHIS (41) with a strong constitutive PMA1 promoter. The protease-deficient *S. cerevisiae* yeast strain BJ5457 was used for overexpression. Procedures for overexpression and plasma membrane isolation were performed as described in ref. 22. Plasma membranes (2 mg/ml) were solubilized at 4°C, using 1% *n*-decyl-β-D-maltoside (DM) for 2 h in the presence of 20 mM sodium phosphate buffer (pH 8.0), 500 mM NaCl, and 1 μM DDT. Insoluble membranes were removed by centrifugation at 100,000 $\times$ *g* for 1 h, using the Type 45 Ti rotor (Beckman Coulter). The supernatant containing TRPV1 was added to an affinity column of CNBr-activated Sepharose 4B coupled to 1D4 antibody (2 ml, 3–4 mg of Ab/ml) (42), and after washing with 20 mM sodium phosphate buffer, 500 mM NaCl, 1 μM DDT, 10% glycerol, and 0.1% DM, protein was eluted by adding 0.1 mg/ml of 1D4 peptide into the washing buffer. Purified protein was resolved by electrophoresis on a 4–20% linear gradient SDS-polyacrylamide gel (Invitrogen) and transferred to a supported nitrocellulose membrane. The presence of TRPV1 was assayed by using 1D4 antibody and detected by chemiluminescence (Pierce). Polyacrylamide gels were Coomassie blue-stained (Pierce) to verify the presence of purified proteins. Protein concentration was determined by using the BCA method (Pierce). Size-exclusion chromatography analysis was performed by using a Superdex 200 HiLoad 16/60 (GE Healthcare).

Fluorescence-Based Flux Assays. TRPV1 purified protein was dialyzed in the presence of phospholipids and 5 mM Ca^{2+} to prepare unilamellar vesicles, Ca^{2+} external to the vesicles was rapidly removed by gel filtration, and then the vesicle suspension was treated with a "calcium sponge" resin to reduce contaminating metal ions to low nanomolar levels (25). A fluorescent Ca^{2+}-indicator dye, Fura-2 (pentasodium salt; Invitrogen), and ligands were prepared in metal-free form by using the same resin. Vesicles that contain TRPV1

protein and 5 mM internal Ca^{2+} were transferred into 4-ml cuvettes that contained 2–4 μM metal-free Fura-2 and a small stir bar. The cuvette was placed in the chamber of a spectrofluorimeter fitted with a magnetic stirrer. The emission at 510 nm was continuously recorded while agonist RTX was added directly to the cuvette, and then the excitation spectrum was recorded. The decrease in fluorescence at 380 nm and the increase at 340 nm were used to detect calcium released from the vesicles. After RTX (50 nM) addition, ionomycin (2 μM) was added to determine the total vesicular Ca^{2+}. Phospholipids were quantified as inorganic phosphate after hydrolysis to give a ratio of 2.26×10^5 mol lipid per mol TRPV1 tetramer. The average vesicle surface area was determined from the root-mean-square diameter of vesicles imaged in ice (78.7 nm, $n = 66$). Using an average lipid surface area of 75 $Å^2$, and assuming equal areas of both leaflets, there were 51,930 phospholipids per vesicle and 0.230 channels per vesicle. For a Poisson distribution, the fraction of vesicles with at least one channel is $1 - \exp(-0.230) = 0.205$.

Electron Microscopy and Image Analysis. The purified TRPV1 channel was embedded in a thin layer of ice on a holey carbon grid by using standard procedures (43). Commercially supplied Quantifoil grids coated with a ''holey film'' were used. They were coated with a thin continuous carbon film. The sample was quick-frozen by using a robotic instrument designed for this purpose, the Vitrobot (FEI). Frozen-hydrated TRPV1 channel specimens were imaged by using a JEM2010F electron microscope operated at 200 kV and −176°C. Images were recorded at effective magnification of 82,873 on a Gatan 4k × 4k CCD camera with an electron dose of ≈15–20 $e^-/Å^2$ per image frame. Image processing and 3D reconstruction were performed by using the EMAN software package (26). The reconstruction from boxed particles (13,592) extracted from CCD images, spanning a range of defocus values from 1.6 to 4.9 μm, was computed by using EMAN with appropriate contrast transfer function corrections.

Image Processing and Three-Dimensional Reconstruction. Particles were selected manually and boxed by using the BOXER routine (26). The particles were initially aligned by using a reference-free procedure in EMAN (26), and initial classes were sorted based on statistical criteria and averaged. A Fourier common lines procedure was used to determine the relative orientations of the class-average images, and an initial 3D model was generated. This initial model was then used to begin an iterative process of model-based alignment, classification, averaging, reconstruction of a new model, realignment using the new model, etc. In each cycle of this procedure, the current model was used to generate projections over a full range of Euler angles at user-defined angular resolution (7° steps). This cycle was repeated until the model converged, i.e., did not change significantly from one round to the next, as monitored by the Fourier shell correlation, which fell to a criterion value of 0.5 at a resolution of 19 Å after convergence for correlations between both successive iterations and arbitrarily divided halves of the data (see Fig. S3). To evaluate model bias, the structure was re-refined from randomly generated starting models, with and without imposed symmetries (from C1 to C4), and the results were compared. Projections of the models under C2 and C4 symmetry agreed well with each other and with the class averages (99 classes for C4 and 199 classes for C4; see Figs. S2 and S4), lending support for the validity of the fourfold symmetric model.

ACKNOWLEDGMENTS. We thank the staff of the National Center for Macromolecular Imaging for use of facilities and technical advice, Alecia K. Gross for advice on purification, and Burgess N. Christensen for support of the early stages of this project. This work was supported by National Institutes of Health Grants P41-RR02250, R01-EY07981, R01-GM072804, P01-GM99116, and T90-DK071505, and by Welch Foundation Grant Q-0035.

1. Cosens DJ, Manning A (1969) Abnormal electroretinogram from a Drosophila mutant. *Nature* 224:285–287.
2. Montell C, Rubin GM (1989) Molecular characterization of the Drosophila trp locus: A putative integral membrane protein required for phototransduction. *Neuron* 2:1313–1323.
3. Montell C (2005) The TRP superfamily of cation channels. *Sci STKE* 272:re3.
4. Nilius B, Voets T (2005) TRP channels: A TR(I)P through a world of multifunctional cation channels. *Pflügers Arch* 451:1–10.
5. Voets T, Talavera K, Owsianik G, Nilius B (2005) Sensing with TRP channels. *Nat Chem Biol* 1:85–92.
6. Dhaka A, Viswanath V, Patapoutian A (2006) Trp ion channels and temperature sensation. *Annu Rev Neurosci* 29:135–161.
7. Minke B, Cook B (2002) TRP channel proteins and signal transduction. *Physiol Rev* 82:429–472.
8. Clapham DE (2003) TRP channels as cellular sensors. *Nature* 426:517–524.
9. Caterina MJ, *et al.* (1997) The capsaicin receptor: A heat-activated ion channel in the pain pathway. *Nature* 389:816–824.
10. Tominaga M, *et al.* (1998) The cloned capsaicin receptor integrates multiple pain-producing stimuli. *Neuron* 21:531–543.
11. Caterina MJ, *et al.* (2000) Impaired nociception and pain sensation in mice lacking the capsaicin receptor. *Science* 288:306–313.
12. Caterina MJ, Julius D (2001) The vanilloid receptor: A molecular gateway to the pain pathway. *Annu Rev Neurosci* 24:487–517.
13. Tominaga M, Julius D (2000) Capsaicin receptor in the pain pathway. *Jpn J Pharmacol* 83:20–24.
14. Owsianik G, Talavera K, Voets T, Nilius B (2006) Permeation and selectivity of TRP channels. *Annu Rev Physiol* 68:685–717.
15. Niemeyer BA (2005) Structure-function analysis of TRPV channels. *Naunyn-Schmiedeberg's Arch Pharmacol* 371:285–294.
16. Kedei N, *et al.* (2001) Analysis of the native quaternary structure of vanilloid receptor 1. *J Biol Chem* 30:28613–28619.
17. Sokolova O, *et al.* (2003) Conformational changes in the C terminus of Shaker K^+ channel bound to the rat $Kv\beta 2$-subunit. *Proc Natl Acad Sci USA* 100:12607–12612.
18. Sokolova O (2004) Structure of cation channels, revealed by single particle electron microscopy. *FEBS Lett* 564:251–256.
19. Sokolova O, Kolmakova-Partensky L, Grigorieff N (2001) Three-dimensional structure of a voltage-gated potassium channel at 2.5 nm resolution. *Structure* 9:215–220.
20. Higgins MK, Weitz D, Warne T, Schertler GF, Kaupp UB (2002) Molecular architecture of a retinal cGMP-gated channel: The arrangement of the cytoplasmic domains. *EMBO J* 21:2087–2094.
21. Chiu PL, *et al.* (2007) The structure of the prokaryotic cyclic nucleotide-modulated potassium channel MloK1 at 16 Å resolution. *Structure* 15:1053–1064.
22. Moiseenkova VY, Hellmich HL, Christensen BN (2003) Overexpression and purification of the vanilloid receptor in yeast (Saccharomyces cerevisiae). *Biochem Biophys Res Commun* 310:196–201.
23. Molday RS, MacKenzie D (1983) Monoclonal antibodies to rhodopsin: Characterization, cross-reactivity, and application as structural probes. *Biochemistry* 22:653–660.
24. MacKenzie D, Arendt A, Hargrave P, McDowell JH, Molday RS (1984) Localization of binding sites for carboxyl terminal specific anti-rhodopsin monoclonal antibodies using synthetic peptides. *Biochemistry* 23:6544–6549.
25. Meyer T, Wensel T, Stryer L (1990) Kinetics of calcium channel opening by inositol 1,4,5-trisphosphate. *Biochemistry* 29:32–37.
26. Ludtke SJ, Baldwin PR, Chiu W (1999) EMAN: Semiautomated software for high-resolution single-particle reconstructions. *J Struct Biol* 128:82–97.
27. Long SB, Campbell EB, MacKinnon R (2005) Crystal structure of a mammalian voltage-dependent Shaker family K^+ channel. *Science* 309:897–903.
28. Ludtke SJ, Serysheva II, Hamilton SL, Chiu W (2005) The pore structure of the closed RyR1 channel. *Structure* 13:1203–1211.
29. Serysheva II, *et al.* (2003) Structure of the type 1 inositol 1,4,5-trisphosphate receptor revealed by electron cryomicroscopy. *J Biol Chem* 278:21319–21322.
30. Doyle DA, *et al.* (1998) The structure of the potassium channel: Molecular basis of K^+ conduction and selectivity. *Science* 280:69–77.
31. Jiang Y, *et al.* (2003) X-ray structure of a voltage-dependent K^+ channel. *Nature* 423:33–41.
32. Dutzler R, Campbell EB, Cadene M, Chait BT, MacKinnon R (2002) X-ray structure of a ClC chloride channel at 3.0 Å reveals the molecular basis of anion selectivity. *Nature* 415:287–294.
33. Jiang Y, *et al.* (2002) Crystal structure and mechanism of a calcium-gated potassium channel. *Nature* 417:515–522.
34. Jin X, Touhey J, Gaudet R (2006) Structure of the N-terminal ankyrin repeat domain of the TRPV2 ion channel. *J Biol Chem* 35:25006–25010.
35. McCleverty CJ, Koesema E, Patapoutian A, Lesley SA, Kreusch A (2006) Crystal structure of the human TRPV2 channel ankyrin repeat domain. *Protein Sci* 15:2201–2206.
36. Lishko PV, Procko E, Jin X, Phelps CB, Gaudet R (2007) The ankyrin repeats of TRPV1 bind multiple ligands and modulate channel sensitivity. *Neuron* 54:905–918.
37. Mio K, *et al.* (2007) The TRPC3 channel has a large internal chamber surrounded by signal sensing antennas. *J Mol Biol* 367:373–383.
38. Mio K, Ogura T, Hara Y, Mori Y, Sato C (2005) The non-selective cation-permeable channel TRPC3 is a tetrahedron with a cap on the large cytoplasmic end. *Biochem Biophys Res Commun* 333:768–777.
39. Maruyama Y, *et al.* (2007) Three-dimensional reconstruction using transmission electron microscopy reveals a swollen, bell-shaped structure of transient receptor potential melastatin type 2 cation channel. *J Biol Chem* 282:36961–36970.
40. Mio K, *et al.* (2007) The motor protein prestin is a bullet-shaped molecule with inner cavities. *J Biol Chem* 283:1137–1145.
41. Figler RA, Omote H, Nakamoto RK, Al-Shawi MK (2000) Use of chemical chaperones in the yeast Saccharomyces cerevisiae to enhance heterologous membrane protein expression: High-yield expression and purification of human P-glycoprotein. *Arch Biochem Biophys* 376:34–46.
42. Yu H, Oprian DD (1999) Tertiary interactions between transmembrane segments 3 and 5 near the cytoplasmic side of rhodopsin. *Biochemistry* 38:12033–12040.
43. Dubochet J, *et al.* (1988) Cryo-electron microscopy of vitrified specimens. *Q Rev Biophys* 21:129–228.